Historical change of El Niño properties sheds light on future changes of extreme El Niño

Bin Wang[a,b,1], Xiao Luo[a], Young-Min Yang[a,b], Weiyi Sun[c,d,e], Mark A. Cane[f], Wenju Cai[g,h], Sang-Wook Yeh[i], and Jian Liu[c,d,e]

[a]Department of Atmospheric Sciences and International Pacific Research Center, University of Hawaii, Honolulu, HI 96822; [b]Earth System Modeling Center, Nanjing University of Information Science and Technology, 210044 Nanjing, China; [c]Key Laboratory for Virtual Geographic Environment, Ministry of Education, Nanjing Normal University, 210023 Nanjing, China; [d]State Key Laboratory Cultivation Base of Geographical Environment Evolution of Jiangsu Province, Nanjing Normal University, 210023 Nanjing, China; [e]Jiangsu Center for Collaborative Innovation in Geographical Information Resource Development and Application, School of Geography Science, Nanjing Normal University, 210023 Nanjing, China; [f]Department of Earth and Environmental Sciences, Lamont–Doherty Earth Observatory of Columbia University, Palisades, NY 10964; [g]Institute for Advanced Ocean Studies, Qingdao National Laboratory for Marine Science and Technology, 266003 Qingdao, China; [h]Centre for Southern Hemisphere Oceans Research, CSIRO Ocean and Atmosphere, Hobart 7004, Australia; and [i]Department of Marine Science and Convergent Technology, Hanyang University, 15588 Ansan, Korea

El Niño's intensity change under anthropogenic warming is of great importance to society, yet current climate models' projections remain largely uncertain. The current classification of El Niño does not distinguish the strong from the moderate El Niño events, making it difficult to project future change of El Niño's intensity. Here we classify 33 El Niño events from 1901 to 2017 by cluster analysis of the onset and amplification processes, and the resultant 4 types of El Niño distinguish the strong from the moderate events and the onset from successive events. The 3 categories of El Niño onset exhibit distinct development mechanisms. We find El Niño onset regime has changed from eastern Pacific origin to western Pacific origin with more frequent occurrence of extreme events since the 1970s. This regime change is hypothesized to arise from a background warming in the western Pacific and the associated increased zonal and vertical sea-surface temperature (SST) gradients in the equatorial central Pacific, which reveals a controlling factor that could lead to increased extreme El Niño events in the future. The Coupled Model Intercomparison Project phase 5 (CMIP5) models' projections demonstrate that both the frequency and intensity of the strong El Niño events will increase significantly if the projected central Pacific zonal SST gradients become enhanced. If the currently observed background changes continue under future anthropogenic forcing, more frequent strong El Niño events are anticipated. The models' uncertainty in the projected equatorial zonal SST gradients, however, remains a major roadblock for faithful prediction of El Niño's future changes.

El Niño onset | El Niño diversity | El Niño onset regime shift | future projection of extreme El Niño

The intensity change of El Niño under increased greenhouse warming is of great societal concern, yet the projections of climate models continue to give no clear information on it (1, 2). Besides the model approach, investigating and understanding how El Niño properties have changed in the context of the 20th century's global warming may shed light on El Niño's future change. In particular, this is the case if such an effort can reveal the controlling factors that lead to more frequent occurrence of large-amplitude El Niño events.

El Niño events have been classified as eastern Pacific (EP) and central Pacific (CP) El Niño based on the location of the maximum warming (3–10). This classification, however, does not distinguish strong El Niño from moderate ones, although strong El Niño usually exhibits an EP pattern (11), making it difficult to project future change of El Niño intensity. Objective delineation of El Niño-Southern Oscillation (ENSO) diversity on a firm physical basis and using long records is required to distinguish the strong and moderate events and to understand the physics governing changing ENSO properties.

Three Types of Dynamically Distinguished El Niño Events

Different from past classification schemes, we delineate El Niño events based on their evolution from the preonset to mature phases, including initiation, development, propagation, and intensity. A nonlinear K-means cluster analysis (12) (*SI Appendix, Method*) is applied to the evolution of equatorial sea-surface temperature anomalies (SSTAs) in 33 El Niño years during the period of 1901 through 2017 when reanalysis data are more reliable (*SI Appendix, Method*). The analysis uncovers 4 physically meaningful clusters. Fig. 1 shows the composite spatial–temporal structures of their SSTAs. The 4 composite patterns generally represent well the individual events within respective composite groups, although the strong basin-wide (SBW) group is less homogeneous before the onset (*SI Appendix*, Fig. S1).

Clusters 1–3 (Fig. 1 *A–C*) depict the first-year El Niño events and they are, respectively, SBW, "moderate eastern Pacific" (MEP), and "moderate central Pacific" (MCP) events. Cluster 4 depicts 2 consecutive El Niño years (Fig. 1*D*) and so is named a "successive" El Niño. Table 1 summarizes characteristics of the SBW, MCP, and MEP El Niños shown in Figs. 1 and 2.

Significance

How the magnitude of El Niño will change is of great societal concern, yet it remains largely unknown. Here we show analysis of how changing El Niño properties, due to 20th century climate change, can shed light on changes to the intensity of El Niño in the future. Since the 1970s, El Niño has changed its origination from the eastern Pacific to the western Pacific, along with increased strong El Niño events due to a background warming in the western Pacific warm pool. This suggests the controlling factors that may lead to increased extreme El Niño events in the future. If the observed background changes continue under future anthropogenic forcing, more frequent extreme El Niño events will induce profound socioeconomic consequences.

EARTH, ATMOSPHERIC, AND PLANETARY SCIENCES

Fig. 1. Composite evolution of the equatorial Pacific SST anomalies in 4 types of El Niño: (*A*) strong basin-wide (SBW), (*B*) moderate EP (MEP), (*C*) moderate CP (MCP), and (*D*) successive El Niño events. Shown are composite longitude–time diagrams of the equatorial SSTA (in units of °C) averaged between 5°S and 5°N. The green lines outline the propagation tracks of maximum SSTAs. The stippling denotes the regions where the signal (group mean) is larger than noise (the SD of each member from the group mean). The time ordinate is from October of the year prior to the El Niño year (–1) to the February after the El Niño year (1). The merged Hadley Centre Sea Ice and Sea Surface Temperature data set (HadISST) and Extended Reconstructed Sea Surface Temperature v5 (ERSST5) data from 1901 to 2017 were used after removing insignificant linear trends.

The strong SBW El Niños (5 events) are distinguished by their extraordinary intensity (maximum SSTA > 2.5 °C) (*SI Appendix,* Fig. S1). The warming starts in the western Pacific and initially propagates eastward, followed by a distinctive basin-wide development in the northern spring, reaching a maximum amplitude around 120°W in December (Fig. 1*A*). A unique feature of SBW events is the pronounced westerly anomalies occurring during the previous winter and spring over the western Pacific (130°E-160°W) (Fig. 2*A*), possibly reflecting frequent westerly wind bursts (WWBs) events (13, 14). The strong anomalous westerlies, with a maximum intensity at 160°E, are coupled with convective and warm SST anomalies near the dateline (*SI Appendix,* Fig. S2*A*) and initiate an eastward displacement of the warm pool by advective processes in the CP (13–15). In addition, the anomalous westerlies in the far western Pacific lead the

positive thermocline and SST anomalies in the far EP by about 2 to 3 mo (Fig. 2*A*), suggesting that the anomalous westerlies trigger EP warming by exciting eastward-propagating downwelling Kelvin waves (13–15). As a result, the strong events are characterized by a ubiquitous basin-wide warming.

The MEP El Niños (12 events) are notably preceded by La Niña events (Fig. 1*B*). The warming originates from the far EP, and then propagates westward and reaches a maximum intensity around 130°W in December (Fig. 1*B*). The onset occurs around July in the NINO 3 region, coupled with convective anomalies in the CP and westerly anomalies in the western Pacific (*SI Appendix,* Fig. S2*B*). An exclusive feature of the MEP Niño is the dramatic reversal of easterly anomalies from February to June over the central-western Pacific, which is accompanied by a sudden relaxation of thermocline slope and thermocline deepening in the EP (Fig. 2*B*), triggering a rapid EP warming (Fig. 2*B*, 7–9). The warming propagates westward because an SSTA-induced positive wind-stress anomaly promotes warming to its west by suppressing upwelling, deepening the thermocline, and reducing evaporative cooling.

In contrast, the MCP El Niños (8 events) begin with a prolonged mild warming in the western Pacific (~165°E), move and expand eastward, reaching a maximum in the CP (Fig. 1*C*). The onset occurs around July with maximum warming at the dateline, which is tightly coupled with convective and westerly anomalies located slightly to the west of the dateline (*SI Appendix,* Fig. S2*C*). Compared with SBW events, the westerly anomaly is much weaker and occurs later after April (Fig. 2*C*). The MCP El Niño develops near the dateline where the climatological SST gradient is large. The anomalous westerlies associated with the MCP events are strong over the central-western Pacific (Fig. 2*C*), favoring a strong zonal advective feedback (5–9).

The 3 types of El Niño onset identified by the cluster analysis involve distinctive dynamical processes. This assertion is supported by an ocean mixed-layer heat budget analysis (*Method*). As shown in Table 2, during June, July, and August, the zonal advective feedback is much stronger in the MCP event (0.15 °C month^{-1}) than in the MEP event (0.06 °C month^{-1}); on the other hand, the thermocline feedback is stronger in the MEP event (0.08 °C month^{-1}) than in the MCP event (0.05 °C month^{-1}). Interestingly, the zonal advective (0.35 °C month^{-1}), thermocline (0.23 °C month^{-1}), and upwelling (0.26 °C month^{-1}) feedbacks are all strong in the SBW events, leading to their distinctive large amplitude. In addition, over the CP, the zonal advective feedback is stronger in all 3 cases, whereas over the EP, the thermocline feedback is stronger than the zonal advective feedback in the MEP and SBW events. The mixed-layer heat budget results may change somewhat when another ocean reanalysis dataset is used (16), but the qualitative conclusions are unlikely to be changed.

Comparing with the existing classification of El Niño events, the present categorization distinguishes between the strong and moderate El Niño events and also between the first-year and successive El Niño. The strong events originate from the western Pacific (similar to the MCP-El Niño) but mature in the EP (similar to the MEP-El Niño) and they involve both the zonal advective feedbacks in the CP (as in the MCP-El Niño) and the thermocline feedback in the EP (as in the MEP-El Niño). Classification based

Table 1. Comparison of the characteristics of the MCP, SBW, and MEP events

Phase	MCP	SBW	MEP
Preonset	Prolonged weak warming in WP	Initial warming and strong WWBs in WP	La Niña conditions
Onset	Summer at CP	Spring, basin-wide	Summer at EP
Development processes	Zonal advective feedback	Zonal advective and thermocline/upwelling feedbacks	Thermocline feedback
SSTA propagation	Eastward	Eastward at onset	Westward
Mature	~160°W (1.0 to 2.5 K)	~120°W (>2.5 K)	~140°W (1.0–2.5 K)

Fig. 2. Composite evolution of the surface zonal wind and thermocline anomalies associated with three types of the first-year El Niño: (*A*) strong basin-wide (SBW), (*B*) moderate EP (MEP), and (*C*) moderate CP (MCP) El Niño events. Contours (in units of meters per second) denote 1,000 hPa zonal wind anomaly and color shading (in units of meters) denotes thermocline depth anomaly. The stippling denotes the regions where the signal (group mean) is larger than noise (the SD of each member from the group mean) for zonal winds. The thermocline depth is defined by the depth of 20 °C isotherm. Linearly detrended data were used. For the zonal wind, the merged National Centers for Environmental Prediction (NCEP) and EC data during 1901 through 2017 were used. For the thermocline depth the merged Simple Ocean Data Assimilation (SODA) and Global Ocean Data Assimilation System (GODAS) data were used (*Methods*).

Fig. 3. Changing El Niño types from 1901 to 2017. The ONI bars represent the SSTA averaged in the NINO3.4 region (5°S–5°N, 120°W–170°W) and during the northern winter season from October to the next February (ONDJF). An El Niño event is defined by ONDJF ONI equal to or greater than 0.6 °C (the dashed line). The 33 El Niño events are shown in different color bars: SWB (black), MEP (blue), MCP (red), and successive (yellow), respectively. Gray bars mark the remaining warm neutral years.

only on the locations of the maximum warming in the mature phase would mix the SBW events with the MEP events. The present analysis finds that SBW and MCP events share a common western Pacific origin and 3 super SBW events occur in the period that MCP events prevail. On the other hand, SBW events are distinguished from the MCP events by the prominent westerly anomalies in the western-CP occurring from January to April (Fig. 2). During the El Niño developing summer, the SSTAs associated with 3 types of El Niño onset show distinct differences in both the locations and intensities of maximum SSTA; thus, their impacts on global land precipitation are expected to be distinctive.

Change of the El Niño Onset under the 20th Century's Climate Change

The change of El Niño properties under the 20th century's climate change remains a gap in our knowledge. The classification reveals that all of MEP events occurred before the late 1970s, while all of MCP events occurred after the late 1970s (Fig. 3). Three out of 5 SBW events, namely the 3 extreme El Niño events (1982 to 1983, 1997 to 1998, and 2015 to 2016) all occurred after the late 1970s. Note that the 3 extreme events occurred in the years adjacent to MCP El Niños, not MEP El Niños. Thus, since the late 1970s, the El Niño onset changes from an EP origin to a western Pacific origin with intermittent SBW events having occurred more frequently in coincidence with MCP events. This is likely a consequence of sharing their common origin in the

western Pacific. Similar to MCP events, the recent extreme El Niño events have all originated from the western Pacific and initially propagated eastward. The change of the El Niño onset and propagation patterns since the late 1970s was documented in the 1990s (17) and has continued to date (Fig. 3).

The change of El Niño onset regime around the late 1970s is statistically significant. Table 3 shows a 2-way table for testing the statistical significance of the changes of the frequency of occurrence of the 3 types of El Niño before and after the late 1970s. The χ^2 test indicates that the regime shift around 1978 is significant at the 99.9% confidence level.

What has caused the observed change of El Niño regimes? It has been recognized that decadal variations of the background state may have profound impacts on ENSO behavior (17–19). Fig. 4 shows the equatorial background-state changes. The equatorial western Pacific has experienced a significant warming trend coincident with global warming (Fig. 4*A*) but the central-EP has not. As such, the equatorial zonal SST gradient around the dateline, defined by SSTA (5°S–5°N,135°E–165°E) minus SSTA (5°S–5°N,165°W–135°W), has been enhanced since 1980. Consistent with the increased westward SST gradient, the easterly trade winds near the dateline (150°E–150°W) have also strengthened and the thermocline has shallowed in the past 4 decades with the largest shoaling occurring in the NINO 3.4 (120°W–170°W) region (Fig. 4*B*), which results from the enhanced easterlies in the CP and the basin-wide wind anomalies (20). This thermocline shoaling together with surface layer warming has substantially increased the vertical temperature gradients (upper-ocean stratification) across the equatorial Pacific.

These changes in the background conditions over the past 4 decades are arguably favorable for the occurrence of MCP and SBW El Niño events. First, the warming in the western Pacific increases the zonal SST gradients across the dateline, and thus enhances the zonal advective feedback process, which is conducive to El Niño being initiated in the NINO 4 (160°E–150°W) region. This explains why MCP and SBW events tend to occur coincidently and predominantly after the late 1970s. To support this argument, we show, in Fig. 5, that the observed NINO4 SSTA

Table 2. Ocean mixed-layer heat budget analysis of 3 types of El Niño during June, July, and August of the El Niño developing year over the equatorial central-EP (5°S–5°N, 160°W–80°W)

Region	ENSO types	$-u'\frac{\partial \bar{T}}{\partial x}$	$-\bar{u}\frac{\partial T'}{\partial x}$	$-u'\frac{\partial T'}{\partial x}$	$-w'\frac{\partial \bar{T}}{\partial z}$	$-\bar{w}\frac{\partial T'}{\partial z}$	$-w'\frac{\partial T'}{\partial z}$
160°W–80°W	SBW	**0.35**	−0.06	−0.06	0.26	**0.23**	−0.11
	MEP	0.06	0.00	−0.01	−0.01	**0.08**	0.00
	MCP	**0.15**	−0.04	0.01	0.01	0.05	−0.01

The units are °C month^{-1}. The dominant feedback in each type of El Niño is marked bold. The terms $-u'\partial\bar{T}/\partial x$, $-\bar{w}\partial T'/\partial z$, and $-w'\partial\bar{T}/\partial z$ represent the zonal advective feedback, thermocline feedback, and upwelling feedback, respectively.

Table 3. Contingent (2-way) table showing the regime change of El Niño between pre-1978 and post-1978

	MCP	SBW	MEP	Total
Pre-1978	0	2	12	14
Post-1978	8	3	0	11
Total	8	5	12	25

Shown are the numbers of the 3 types of El Niño events. The degree of freedom equals to 2 and chi square value equals 20.1 (*P* < 0.001).
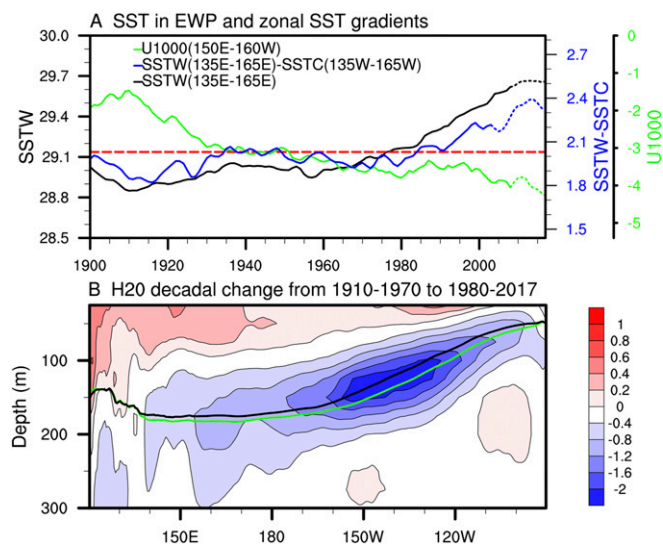
Fig. 4. Change of the background state in the equatorial Pacific. (*A*) Time series of background-state SST averaged over the equatorial WP (SSTW, 5°S–5°N, 135°E–165°E) and the zonal SST gradients measured by SST (5°S–5°N, 135°E–165°E) minus SST (5°S–5°N, 165°W–135°W) (SSTW-SSTC), and the 1,000-hPa background zonal wind anomalies averaged over the CP (5°S–5°N, 150°E–160°W) (U1,000). The SSTW and zonal wind are 21-y running time series, while SSTW-SSTC is a 31-y running mean. The dotted lines in the last 10 to15 y are not reliable as they are not full 31- or 21-y running means. (*B*) Changes in the equatorial ocean temperature (the upper 300 m) climate between the MEP epoch (1910 through 1970) and MCP epoch (1980 through 2017) (color, °C). The thermoclines in the MEP epoch (green) and CP (black) epoch are also shown. The ocean stratification, defined as the difference between the mean temperature over the upper 75 m and the temperature at 100 m averaged over 150°E–140°W, increases from 0.9 °C during MEP epoch to 1.5 °C during the MCP epoch. The merged SST and merged NCEP zonal winds data from 1871 through 2017 were used.

during the El Niño onset phase (April through August) indeed increases with the increasing mean-state zonal SSTA gradient measured by SSTA (5°S–5°N, 135°E–165°E) minus SSTA (5°S–5°N, 135°W–165°W) with a significant correlation coefficient $r = 0.85$ ($P < 0.01$). To a large extent, the explanation here is also consistent with the results obtained from coupled climate model experiments (21), in which an initial warming in the western Pacific is associated with strong zonal gradients of mean SST and trade winds in the equatorial CP. Second, the western Pacific warming provides favorable conditions for the Madden–Julian Oscillation (22) events to move into the western Pacific more frequently (23), increasing the frequency of WWBs and thereby the probability of occurrence of SBW events. In addition, the increased vertical temperature gradients strengthen the thermocline feedback, favoring occurrence of SBW events.

Implication for the Future Change of El Niño Properties

The aforementioned observational analysis reveals the controlling factors that would lead to increased large-amplitude El Niño events in the future. We hypothesized that more frequent occurrences of SBW and MCP events require an enhanced zonal SST gradient in the CP. We have tested this hypothesis using 8 CMIP5 (Coupled Model Intercomparison Project phase 5) models' historical runs and future projection results (*Methods*). We find that the model results are consistent with the hypothesis derived from the observations. Under anthropogenic forcing-induced warming, the 8 CMIP5 models project different changes in the mean-state zonal equatorial SST gradients measured by the western Pacific (WP) SST (5°S–5°N, 150°–180°E) minus EP SST (5°S–5°N, 120°–150°W) (Fig. 6). As

shown in Fig. 6, when the zonal mean SST gradient increases under the anthropogenic forcing, both the frequency of occurrence and the intensity of the SBW El Niño events increase significantly. This implies that if anthropogenic forcing enhances the SST gradients in the CP as we have observed over the past century, the extreme El Niño events will occur more frequently.

Conclusion and Discussion

In the present work, consideration of the onset and evolution of El Niño events (Figs. 1 and 2) has led to the innovative classification of El Niño diversity, and uncovered an El Niño onset regime change from an EP origin to a western Pacific origin in the late 1970s (Fig. 3). The onset changes and more frequent occurrence of the extreme events in the past 4 decades arise from a background warming in the equatorial WP and the associated enhanced zonal SST gradients in the equatorial CP (Fig. 4). This reveals that a controlling factor that could lead to increased extreme El Niño events in the future is the enhanced mean-state zonal SST gradient in the CP. Observation suggests that increased zonal SST gradients in the CP favor the development of warming in the NINO 4 region (Fig. 5). The CMIP5 models' historical simulations and future projections also indicate that both the frequency and intensity of the strong El Niño events increase significantly with increased mean-state CP zonal SST gradients (Fig. 6).

While the observed background-state changes in the Pacific Ocean are responsible for the changing El Niño properties, the root causes of the observed background changes in the later part of the 20th century remain elusive and the background SST changes also remain uncertain due to differences among SST datasets (24). It could be linked to natural internal variability (25, 26) because, even in the absence of external radiative forcing, coupled general circulation models can generate multi-decadal variations of the mean state and ENSO diversity (27). However, the change of El Niño in the late 1970s coincides with a rapid warming in the Indo-Pacific warm pool, suggesting that the recent rapid global warming may have had an impact on the observed El Niño changes. Note that this recent global warming need not have been due solely to anthropogenic forcing. The forced component of recent tropical SST trends, as given by the ensemble mean of climate model simulations, is much weaker and more spatially homogeneous than the observed SST trend (28). Natural variability may have added significant contributions to the recent warming. While we attribute the El Niño onset
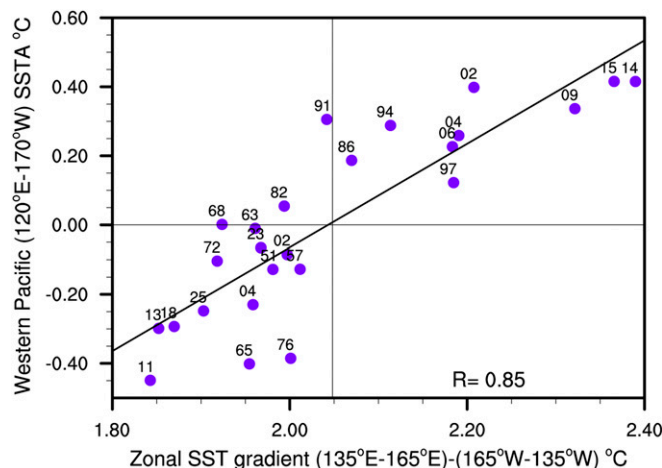
Fig. 5. Relationship between the mean-state zonal SSTA gradient [SSTW(135–165°E) minus SSTC(165–135°W)] and the WP (120°E–170°W) SSTA during the El Niño onset phase from April (0) to August (0). The solid line denotes linear regression ($r = 0.85$). The mean state is defined by the 31-y running mean climatology.
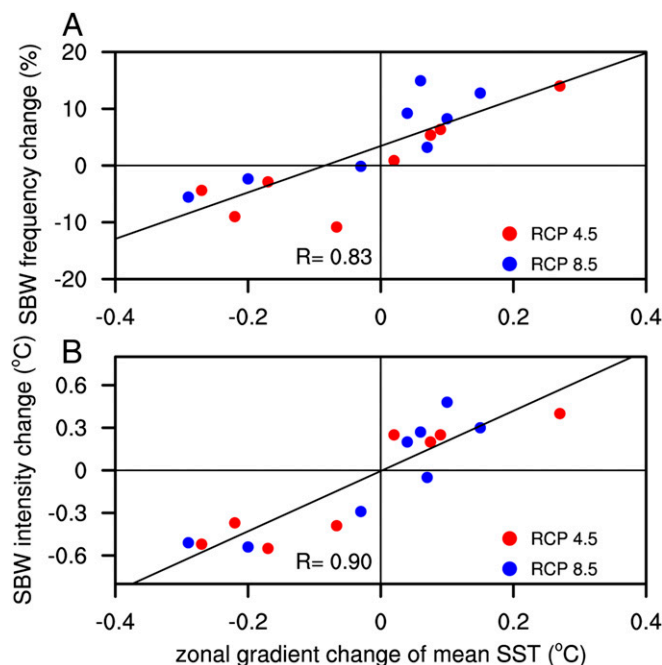
Fig. 6. Dependence of the future change of SBW El Niño events on the change of the mean-state zonal SST gradient measured by the WPSST (5°S–5°N, 150°–180°E) minus EPSST (5°S–5°N, 120°–150°W). (*A*) Change of the frequency, and (*B*) change of the intensity measured by the SST anomalies averaged over (5°S–5°N, 80°W–180°W) and from October (0) to February (1). Eight CMIP5 models were used. Red (blue) dots represent the change values derived from representative concentration pathway (RCP)4.5 (RCP8.5) scenario. Linear regression line is shown by the dotted line with the significant correlation coefficient (R) indicated in each panel.

regime change to the mean SST gradient change, there is an alternative possibility that the mean-state change is affected by the rectification effect of the randomly changing El Niño and La Niña due to their nonlinear asymmetry (25, 29).

The future change of ENSO amplitude is an extremely important issue. Fig. 3 indicates that El Niño amplitude change is primarily determined by the frequency of SBW El Niño events; in addition, SBW events tend to concur with MCP events. More frequent occurrences of SBW and MCP events require enhanced SST gradients in the western-CP which can enhance zonal advective feedback and increase the probability of WWB occurrence in the WP. In addition, increased upper-ocean vertical temperature gradients in the central-EP may favor SBW events by enhancing the thermocline and upwelling feedbacks. If anthropogenic warming produces a mean-state change similar to the recent change, more frequent MCP and strong El Niño events will occur; however, an El Niño-like mean-state change will favor prevailing MEP events, reducing the frequency of extreme El Niño events.

The current generation of models has great difficulty in capturing the El Niño diversity and the projected Pacific mean-state changes are highly uncertain due to models' biases in simulating mean states and ENSO (30, 31). The impact of climate change on the mean east–west gradient of SST in the tropical Pacific has been an issue of some debate. The "weak Walker circulation" theory (32, 33) proposes that the Walker circulation must slow down because the greenhouse-gas-induced warming increases

atmospheric static stability. The weakened Walker circulation, in turn, reduces the east–west SST gradient by a mechanism known as "the Bjerknes feedback." On the other hand, the "ocean dynamical thermostat" theory (34, 35) argues that increased heating at the surface warms SSTs in the west more because the heating in the east is offset by cold upwelling. The increase in SST gradient induces an enhanced pressure gradient and hence a stronger Walker circulation, which in turn enhances the SST gradient. The present work indicates that the uncertainty in the projected equatorial zonal SST gradients currently prohibits faithful prediction of the future change in El Niño. The cluster analysis for delineating ENSO diversity provides a metric for validation and improvement of the capacity of climate models to reproduce the observed ENSO complexity, which is critical for improved ENSO prediction and reduced uncertainties in future projection of ENSO changes.

Methods

Definition of El Niño Years (1901 through 2017). The SST anomaly averaged in the NINO 3.4 region (5°N–5°S, 120°–170°W), known as Oceanic Niño Index (ONI), is averaged for October-November-December-January-February (ONDJF) to identify El Niño years, because ONI has largest variances during ONDJF (*SI Appendix*, Fig. S3*B*). An El Niño year is defined as ONDJF ONI is greater than or equals to 0.6 °C. Using the linearly detrended data, 33 El Niño years are identified.

Cluster Analysis. The K-means cluster analysis (12) uses squared Euclidean distance to measure the "similarity" between each cluster member and the corresponding cluster centroid. The silhouette clustering evaluation criterion was used to evaluate the performance of cluster analysis (*SI Appendix*, Fig. S5). The silhouette value for each member is a measure of the similarity between that member and other members in its own cluster, which ranges from −1 to +1. A high silhouette value indicates that the member is well-matched to its own cluster and poorly matched to its neighboring clusters (36). We used K = 4 clusters as the exemplars of different evolutionary patterns mainly based on physical meanings and its stability.

Ocean Mixed-Layer Heat Budget Equation. The ocean mixed-layer heat budget equation is

$$\frac{\partial T'}{\partial t} = -(V' \cdot \nabla \overline{T} + \overline{V} \cdot \nabla T' + V' \cdot \nabla T') + \frac{Q'_{net}}{\rho C_p H} + R = -\left[\left(\frac{u'\partial \overline{T}}{\partial x} + \frac{\overline{u}\partial T'}{\partial x} + \frac{u'\partial T'}{\partial x}\right)\right.$$
$$\left. + \left(\frac{v'\partial \overline{T}}{\partial y} + \frac{\overline{v}\partial T'}{\partial y} + \frac{v'\partial T'}{\partial y}\right) + \left(\frac{w'\partial \overline{T}}{\partial z} + \frac{\overline{w}\partial T'}{\partial z} + \frac{w'\partial T'}{\partial z}\right)\right] + \frac{Q'_{net}}{\rho C_p H} + R,$$

where *T* denotes the mixed-layer temperature; V = (*u*, *v*, *w*) represents the zonal and meridional currents and upwelling velocities, respectively; The mixed-layer depth *H* is taken as a constant 50 m (29, 37), which is not sensitive to the different mixed-layer thickness in this study, such as H = 30 or 70 m.

For detailed introduction of data and method please refer to *SI Appendix*.

1. M. Collins *et al.*, The impact of global warming on the tropical Pacific Ocean and El Niño. *Nat. Geosci.* **3**, 391–397 (2010).
2. M. Watanabe *et al.*, Uncertainty in the ENSO amplitude change from the past to the future. *Geophys. Res. Lett.* **39**, L20703 (2012).
3. A. Capotondi *et al.*, Understanding ENSO diversity. *Bull. Am. Meteorol. Soc.* **96**, 921–938 (2015).
4. A. Timmermann *et al.*, El Niño-Southern oscillation complexity. *Nature* **559**, 535–545 (2018).
5. K. Ashok, S. K. Behera, S. A. Rao, H. Weng, T. Yamagata, El Niño Modoki and its possible teleconnection. *J. Geophys. Res. Oceans* **112**, C11007 (2007).
6. S.-W. Yeh *et al.*, El Niño in a changing climate. *Nature* **461**, 511–514 (2009).
7. J.-S. Kug, F.-F. Jin, S.-I. An, Two types of El Niño events: Cold tongue El Niño and warm pool El Niño. *J. Clim.* **22**, 1499–1515 (2009).

EARTH, ATMOSPHERIC, AND PLANETARY SCIENCES

8. J.-Y. Yu, H.-Y. Kao, T. Lee, Subtropics-related interannual sea surface temperature variability in the central equatorial Pacific. *J. Clim.* **23**, 2869–2884 (2010).

9. K. Takahashi, A. Montecinos, K. Goubanova, B. Dewitte, ENSO regimes: Reinterpreting the canonical and Modoki El Niño. *Geophys. Res. Lett.* **38**, L10704 (2011).

10. W. Cai *et al.*, Increased variability of eastern Pacific El Niño under greenhouse warming. *Nature* **564**, 201–206 (2018).

11. Y. M. Okumura, ENSO diversity from an atmospheric perspective. *Curr. Clim. Change Rep.* **5**, 245–257 (2019).

12. D. S. Wilks, *Statistical Methods in the Atmospheric Sciences* (Academic, 2011).

13. M. Lengaigne *et al.*, Triggering of El Niño by westerly wind events in a coupled general circulation model. *Clim. Dyn.* **23**, 601–620 (2004).

14. D. Chen *et al.*, Strong influence of westerly wind bursts on El Niño diversity. *Nat. Geosci.* **8**, 339–345 (2015).

15. A. V. Fedorov, S. Hu, M. Lengaigne, E. Guilyardi, The impact of westerly wind bursts and ocean initial state on the development, and diversity of El Niño events. *Clim. Dyn.* **44**, 1381–1401 (2015).

16. L. Chen, T. Li, S. K. Behera, T. Doi, Distinctive precursory air–sea signals between regular and super El Niños. *Adv. Atmos. Sci.* **33**, 996–1004 (2016).

17. B. Wang, Interdecadal changes in El Niño onset in the last four decades. *J. Clim.* **8**, 267–285 (1995).

18. D. Gu, S. G. H. Philander, Interdecadal climate fluctuations that depend on exchanges between the tropics and extratropics. *Science* **275**, 805–807 (1997).

19. A. V. Fedorov, S. G. Philander, Is El Nino changing? *Science* **288**, 1997–2002 (2000).

20. J. Emile-Geay, M. A. Cane, Pacific decadal variability in the view of linear equatorial wave theory. *J. Phys. Oceanogr.* **39**, 203–219 (2009).

21. J. Choi, S.-I. An, J.-S. Kug, S.-W. Yeh, The role of mean state on changes in El Niño's flavor. *Clim. Dyn.* **37**, 1205–1215 (2011).

22. R. A. Madden, P. R. Julian, Detection of a 40–50 day oscillation in the zonal wind in the tropical Pacific. *J. Atmos. Sci.* **28**, 702–708 (1971).

23. H. H. Hendon, C. Zhang, J. D. Glick, Interannual variation of the Madden–Julian oscillation during austral summer. *J. Clim.* **12**, 2538–2550 (1999).

24. C. Deser, A. S. Phillips, M. A. Alexander, Twentieth century tropical sea surface temperature trends revisited. *Geophys. Res. Lett.* **37**, L10701 (2010).

25. M. McPhaden, T. Lee, D. McClurg, El Niño and its relationship to changing background conditions in the tropical Pacific Ocean. *Geophys. Res. Lett.* **38**, L15709 (2011).

26. M. Newman, S. I. Shin, M. A. Alexander, Natural variation in ENSO flavors. *Geophys. Res. Lett.* **38**, L14705 (2011).

27. A. T. Wittenberg, A. Rosati, T. L. Delworth, G. A. Vecchi, F. Zeng, ENSO modulation: Is it decadally predictable? *J. Clim.* **27**, 2667–2681 (2014).

28. C. Deser, A. S. Phillips, Atmospheric circulation trends, 1950–2000: The relative roles of sea surface temperature forcing and direct atmospheric radiative forcing. *J. Clim.* **22**, 396–413 (2009).

29. S.-I. An, F.-F. Jin, Nonlinearity and asymmetry of ENSO. *J. Clim.* **17**, 2399–2412 (2004).

30. Y.-G. Ham, J.-S. Kug, How well do current climate models simulate two types of El Niño? *Clim. Dyn.* **39**, 383–398 (2012).

31. H. Bellenger, É. Guilyardi, J. Leloup, M. Lengaigne, J. Vialard, ENSO representation in climate models: From CMIP3 to CMIP5. *Clim. Dyn.* **42**, 1999–2018 (2014).

32. I. M. Held, B. J. Soden, Robust responses of the hydrological cycle to global warming. *J. Clim.* **19**, 5686–5699 (2006).

33. G. A. Vecchi, B. J. Soden, Global warming and the weakening of the tropical circulation. *J. Clim.* **20**, 4316–4340 (2007).

34. A. C. Clement, R. Seager, M. A. Cane, S. E. Zebiak, An ocean dynamical thermostat. *J. Clim.* **9**, 2190–2196 (1996).

35. K. B. Karnauskas, R. Seager, A. Kaplan, Y. Kushnir, M. A. Cane, Observed strengthening of the zonal sea surface temperature gradient across the equatorial Pacific Ocean. *J. Clim.* **22**, 4316–4321 (2009).

36. L. Kaufman, P. J. Rousseeuw, *Finding Groups in Data: An Introduction to Cluster Analysis* (John Wiley & Sons, 2009).

37. K. Lorbacher, D. Dommenget, P. Niiler, A. Köhl, Ocean mixed layer depth: A subsurface proxy of ocean-atmosphere variability. *J. Geophys. Res. Oceans* **111**, C07010 (2006).